An Observational Study of the First-Order Vorticity Dynamics in a Tropical Easterly Wave

MARY ANN JENKINS

Department of Earth and Atmospheric Science, York University, North York, Ontario, Canada

HAN-RU CHO

Department of Physics, University of Toronto, Toronto, Ontario, Canada

(Manuscript received 31 July 1989, in final form 23 October 1990)

ABSTRACT

GATE Phase III *A*/*B*- and *B*-scale data were analyzed and used to diagnostically test the first-order vorticity equation proposed by Cho et al. The results are given in the form of a composite easterly wave and the analysis shows that the first-order vorticity equation is capable of describing the vorticity dynamics of the composite easterly wave. Cumulus heating produces significant large-scale vertical motion, and it is demonstrated that the effect of cumulus clouds on the large-scale vorticity field is through vortex-tube stretching by cloud-induced vertical motion.

The composite analysis of the first-order vorticity equation also shows that the vorticity dynamics of tropical easterly waves are adequately described by a linearized first-order vorticity equation and dominated by the advection of the perturbed vorticity by the relative zonal mean wind, the advection of the zonal mean vorticity by the perturbed wind, and the vortex-tube stretching induced by cumulus activity. It is explained how, during Phase III of GATE, the westward convergence and eastward divergence of the wave trough observed just above the surface and the appearance of midlevel divergence before and convergence after the passage of the wave trough axis are associated with the vorticity dynamics of tropical easterly waves.

1. Introduction

A first-order vorticity equation applicable to synoptic-scale tropical disturbances, such as easterly waves, was proposed by Cho et al. (1983). The equation is derived from the synoptic-scale vorticity equation with cumulus-cloud effects parameterized according to the scheme by Cho and Cheng (1980). It represents a significant simplification of the complete vorticity equation in which the interactive processes between cumulus clouds and the larger-scale flow need to be parameterized.

Observational studies of cumulus effects on the vorticity dynamics of synoptic-scale tropical disturbances suggest that the interactive processes between clouds and the large-scale flow are complex and significant, with the net effect being a delicate balance between several equally important processes (Yanai and Nitta 1967; Williams and Gray 1973; Reed and Johnson 1974; Ruprecht and Gray 1976; Daggupatty and Sikka 1977; Stevens 1979; Jenkins et al. 1982; Yanai et al. 1982a; Sui and Yanai 1986). The complicacy of the parameterization schemes needed to adequately describe these processes (Reed and Johnson 1974; Johnson 1976, 1977; Nitta 1977; Shapiro 1978; Cho et al. 1979; Cho and Cheng 1980; Shapiro and Stevens 1980; Cho and Clark 1981; Chu et al. 1981; Yanai et al. 1982b, Sui et al. 1989) makes it difficult to directly relate the effects of convective cloud on the observed structure and evolution of the large-scale vorticity field. The proposed first-order vorticity equation is useful in this regard. It identifies the essential interactive processes that affect the temporal and spatial evolution of the large-scale vorticity field and, because of its simplicity, can be used in future theoretical studies of tropical disturbances.

The purpose of this study is to examine the vorticity dynamics of tropical easterly waves implied by the first-order vorticity equation. In the study by Cho et al. (1983), observational data from Phase III (30 August to 18 September 1974) of the Global Atmospheric Research Program (GARP) Atlantic Tropical Experiment (GATE) were used to verify the first-order vorticity dynamics, but their analysis was made only for the trough regions of the easterly waves that passed through the GATE area during Phase III of the experiment. Here the analysis is extended over the entire wavelengths of easterly waves. The composite technique used by Reed et al. (1977) and Thompson et al. (1979)

Corresponding author address: Dr. Mary Ann Jenkins, Dept. of Earth & Atmos. Sciences, Rm. 149, York University, 4700 Keele Street, North York, Ontario M3J 1P3.

is adopted to produce the structure of a typical easterly wave. The vorticity dynamics of the composite easterly wave are then examined in the context of the first-order vorticity equation.

The organization of the paper is as follows. The first-order vorticity equation is presented in the following section. The GATE Phase III dataset and the analysis used to support this study are discussed in section 3. Results of the diagnostic analysis of the first-order vorticity equation are shown in section 4, followed by a discussion of the implications of the first-order theory for the vorticity dynamics of tropical easterly waves in section 5. The paper is concluded by a few remarks in section 6.

2. The first-order vorticity equation

The first-order vorticity equation derived by Cho et al. (1983) is based on the condition that the air flow in the environmental area between cumulus clouds is approximately nondivergent in the tropical atmosphere, independent of the strength of cumulus convection. The condition is discussed in detail by Cho et al. (1983) and is not presented here. If the parameterization scheme proposed by Cho and Cheng (1980) is used to represent the effects of cumulus clouds on the large-scale vorticity field, then the first-order vorticity equation has the form

$$\frac{\partial \bar{\eta}}{\partial t} + \bar{\mathbf{V}} \cdot \nabla \bar{\eta} = \int \frac{\sigma}{\tau_{p'}} dp' (\bar{\eta}_c - \bar{\eta}). \tag{1}$$

Here $\eta = \mathbf{k} \cdot \nabla \times \mathbf{V} + f$ is the vertical component of the absolute vorticity where $\mathbf{k}$ is the unit vector in the vertical direction, ∇ the horizontal gradient operator, $\mathbf{V}$ the horizontal velocity field, and f the Coriolis parameter. The overbar ($\bar{}$) denotes the horizontal large-scale area average and t is time. The vorticity source due to cumulus clouds on the right side of (1) represents the generation of vorticity through the cloud life-cycle effect defined in Cho (1977). The integral $\int (\sigma/\tau_{p'}) dp'$ is the recycling rate, the fractional area recycled by cumulus clouds of maximum cloud-top height p' and lifetime τ, and $\bar{\eta}_c$ the ensemble mean in-cloud vorticity.

Equation (1) describes a balance between the cloud life-cycle effect, a source of vorticity for the cloud environmental vorticity field, and the evolution and advection of the cloud environmental vorticity. The cloud life-cycle effect is the statistical ensemble average of the local time derivative term in the governing equation for cloud-scale motions. It is proportional to the difference between the values of a cloud variable at the end and at the beginning of the cloud's life span. By identifying the area occupied by each cloud and its life span, and the time evolution of cloud variables, it is possible to determine this effect using proxy cloud ensemble data.

Following the parameterization scheme of Cho and Cheng (1980), the first-order vorticity equation can also take the form

$$\frac{\partial \bar{\eta}}{\partial t} + \bar{\mathbf{V}} \cdot \nabla \bar{\eta} = -\bar{\eta}_{CB} \frac{\partial M_c}{\partial p}, \tag{2}$$

where the vorticity source produced by cumulus convection is expressed in terms of the mean vorticity averaged over the cloud boundaries $\bar{\eta}_{CB}$ and the divergence of the total cloud mass flux $\partial M_c/\partial p$. Here M_c is the total cloud mass flux induced by cumulus convection as defined by Cho (1977) and includes both condensation-induced upward motions and evaporation-induced cloud-scale downward motions. According to Cho et al. (1979), if vertical velocities in the cloud environment are very weak, the time rate of change of the cloud vertical vorticity when averaged over the cloud horizontal area is influenced only by the divergence of vortex lines through the cloud boundary. A numerical cloud simulation by Cho and Clark (1981) examined the validity of Cho et al.'s (1979) assumption and found that the governing equation for the mean cloud vorticity can be reduced to this simple relationship. Here it is recognized that the cloud life-cycle effect represents the ensemble mean of the time rate of change of cloud vorticity and is equal to the divergence of vorticity through cloud boundaries.

Again based on the condition described by Cho et al. (1983) that the airflow in the cloud environment is essentially nondivergent, further simplification is introduced to (2) so that

$$\frac{\partial \bar{\eta}}{\partial t} + \bar{\mathbf{V}} \cdot \nabla \bar{\eta} = -\bar{\eta}_{CB} \bar{\delta} \tag{3}$$

where, by reason of mass continuity, $\delta = \nabla \cdot \mathbf{V}$ is the horizontal divergence of the velocity field. Here $\bar{\delta} = \partial M_c/\partial p$ is an expression of the condition used by Cho et al. (1983) to derive the first-order vorticity equation. This form of the first-order vorticity equation implies a direct correspondence between the convergence and divergence of the total cloud mass flux and the evolution of the large-scale vorticity field. Significant large-scale vertical motion is induced in low latitudes only through cumulus heating and, through the mechanism of convective vortex-tube stretching, significant vorticity variations as well. At levels where a net horizontal convergence (or divergence) of the cloud mass flux exists, which is reflected on the synoptic scale as the convergence (or divergence) of the mean wind, a positive (or negative) contribution is made to the total horizontal derivative of vorticity, resulting in a possible increase (or decrease) in the effective angular velocity of the air parcel due to vortex-tube stretching (or shrinking) by cumulus clouds.

3. Data source and analysis

To test whether the first-order vorticity equation accurately describes the vorticity dynamics of synoptic-scale tropical weather systems, A/B- and B-scale upper-air data collected during Phase III of GATE are used. Validated Phase III upper-air temperature, relative humidity, wind speed and direction, and height data were provided on tape by the U.S. World Data Center in Asheville, North Carolina. The method of data analysis was reported in Jenkins et al. (1982). The details of the procedures attempted to assess and eliminate the systematic biases in the height, temperature, and humidity data between A/B- and B-scale ships are also summarized there. A three-hour time interval was used in this analysis. All available ship observations were fitted using a least squares method to a second-order polynomial. For any observation γ it was assumed that

$$\gamma = Ax^2 + By^2 + Cxy + Dx + Ey + F, \quad (4)$$

where x and y are the east–west and north–south coordinates, respectively. The uppercase Roman alphabets of the polynomial are the best-fit coefficients in the least squares sense and were used to analytically determine the needed parameters.

During Phase III of GATE six tropical easterly waves, having originated over western Africa, passed in regular succession across the GATE area. An excellent chronology of these waves is presented and discussed in detail by Thompson et al. (1979). It was decided, rather than study the behavior of the waves individually, to construct a composite easterly wave of these six waves.

Compositing of the data was done as follows. Adopting the classification scheme first introduced by Reed and Recker (1971), each ship sounding was assigned one of eight wave categories in accordance with the wave phase classification given in Thompson et al. (1979). The average of a parameter, term, or sum—whichever was required—for every wave category was then calculated. These wave category means produced a wave composite representing eight wave regions over one wavelength of a tropical easterly wave. Categories [2], [4], [6], and [8] designate regions of maximum northerly winds [N], wave troughs [T], maximum southerlies [S], and wave ridges [R] at the 700-mb level, respectively. Categories [1], [3], [5], and [7] are intermediate regions. To isolate the dynamics of the wave disturbance itself, analysis results are presented as wave components found by subtracting the overall GATE Phase III mean from the composite wave category mean.

4. Consistency check

The vorticity dynamics of the composite easterly wave and the simple vorticity equation are investigated and the results reported in this section. To illustrate plainly the wave structure of each meteorological field, Phase III wave composite fields are displayed as vertical cross sections over one wavelength of the wave. In each vertical cross section are drawn lines representing the trough and ridge axes of the wave, typically the trough (ridge) axis being the region of the wave where the amplitude of vorticity is a maximum (minimum).

The composite results of the effects of convection on the evolution of the large-scale vorticity field are represented simply by wave category means of $\int(\sigma/\tau_{p'})dp'(\bar{\eta}_c - \bar{\eta})$, $\bar{\eta}_{CB}(\partial M_c/\partial p)$, and $\bar{\eta}_{CB}\bar{\delta}$. Unlike a numerical simulation of the vorticity fields associated with convective cloud (e.g., Cho and Clark 1981), observations from Phase III of GATE do not provide the detail necessary to produce directly values for $\int(\sigma/\tau_{p'})dp'(\bar{\eta}_c - \bar{\eta})$, $\bar{\eta}_{CB}(\partial M_c/\partial p)$, and $\bar{\eta}_{CB}\bar{\delta}$ following the definitions by Cho (1977) given in section 2. Rather, the total cloud mass flux M_c and recycling rate $\int(\sigma/\tau_{p'})dp'$ are found from the A/B- and B-scale heat and moisture budgets, respectively, using the diagnostic procedure introduced by Cho (1977). The mean in-cloud vorticity $\bar{\eta}_c$ is also determined diagnostically, using the method of Cheng et al. (1980). The cloud source term in (2) and (3) is difficult to determine exactly because $\bar{\eta}_{CB}$ cannot be found directly from observational data. Therefore the approximation is made that $\bar{\eta}_{CB} = \bar{\eta}$. The choice of $\bar{\eta}_{CB}$ is based on the argument that the vorticity at the cloud boundary must be essentially the same as the mean environmental vorticity for the cloud edge to ever merge with its environment, and the mean environmental vorticity is the same as the mean vorticity (Cho et al. 1979; Cho et al. 1983). It will be seen later that this approximation is qualitatively and, to some extent, quantitatively reliable.

The cross sections of the wave components of the large-scale mean absolute vorticity $\bar{\eta}$ and divergence $\bar{\delta}$ are shown in Figs. 1a,b. Generally, they are similar in magnitude and behavior to the composites of Thompson et al. (1979, Figs. 12 and 13) and Reed et al. (1977, Fig. 8). The ridge and trough axes are nearly vertical below 800 mb, sloping westward above, and the vorticity maximum at the 650-mb level is one category ahead of the surface trough. The wave divergence varies considerably in the vertical, particularly over the trough region. In the lower troposphere, below 750 mb, the most significant convergence occurs just ahead of and above the surface trough; in the middle troposphere, between 750 and 500 mb, relatively strong divergence takes place; and in the upper troposphere, around 200 mb, just above a weak shallow layer of convergence, divergence occurs again. Between 800 and 500 mb, in the middle troposphere, at the level of the African easterly jet, divergence increases as the trough axis approaches and decreases as the ridge axis approaches. An explanation for this behavior is presented in section 5. Above cloud base (~900 mb) and below 300 mb the wave amplitude of divergence is smaller

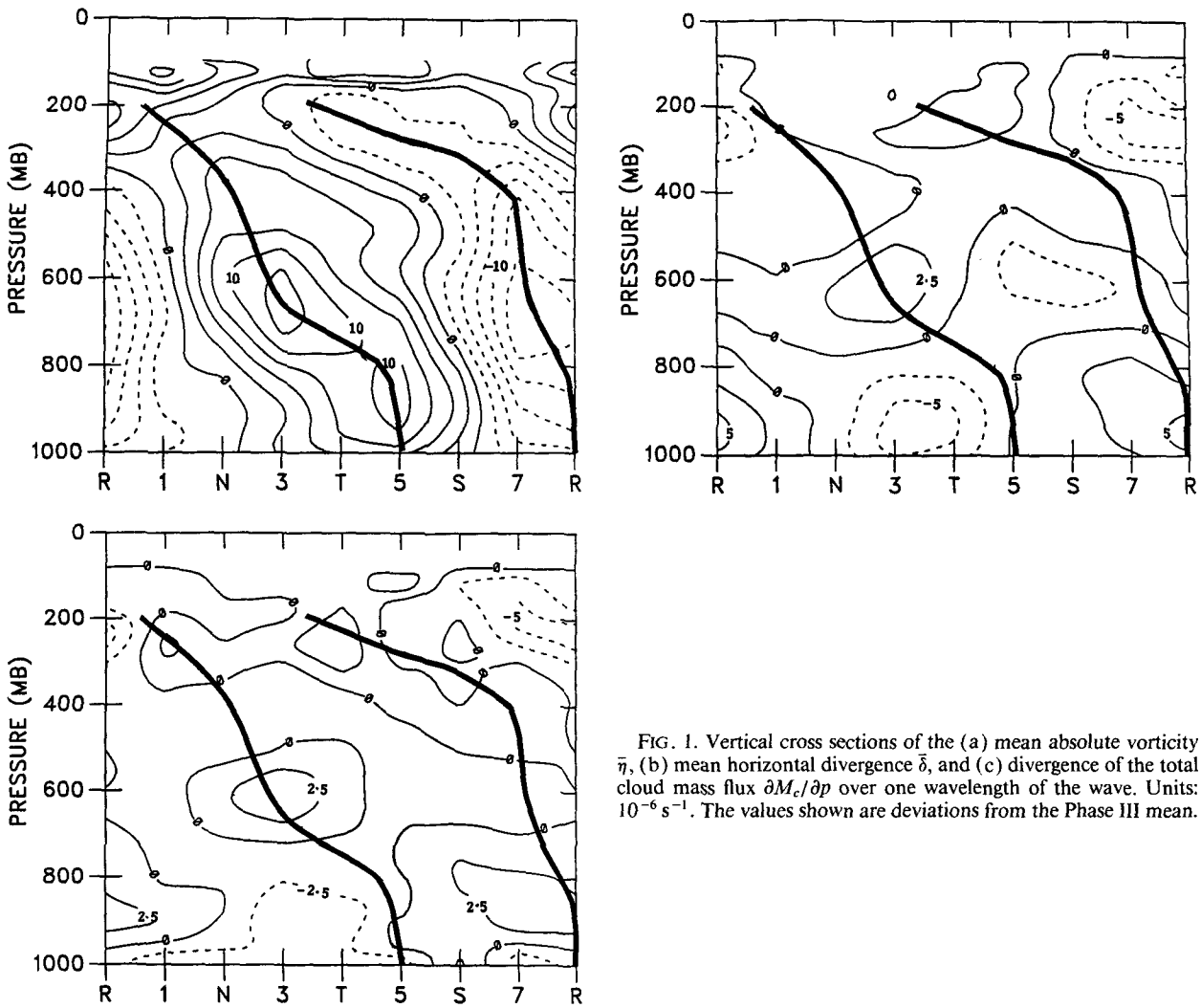

FIG. 1. Vertical cross sections of the (a) mean absolute vorticity $\bar{\eta}$, (b) mean horizontal divergence $\bar{\delta}$, and (c) divergence of the total cloud mass flux $\partial M_c/\partial p$ over one wavelength of the wave. Units: $10^{-6}\ s^{-1}$. The values shown are deviations from the Phase III mean.

in magnitude than that of vorticity by a factor of ~3, indicating that these waves are quasi-nondivergent throughout a substantial depth of the troposphere.

Figures 1b,c demonstrate how similar in behavior the wave components of $\bar{\delta}$ and $\partial M_c/\partial p$ are, an indication of the validity of the condition used by Cho et al. (1983) to systematically simplify the complete vorticity equation. Above cloud base and below 250 mb, with very few exceptions, the behavior and magnitude of $\partial M_c/\partial p$ follow closely that of the mean divergence $\bar{\delta}$. At higher levels above 250 mb however, agreement lessens; the wave behavior of $\partial M_c/\partial p$ is still similar to $\bar{\delta}$, but the wave amplitudes of $\partial M_c/\partial p$ are larger than those of $\bar{\delta}$. Given that the reliability of the data and budget analysis diminishes with height, the larger wave amplitudes of $\partial M_c/\partial p$ in these regions of the wave may not be realistic.

The wave components of $\partial\bar{\eta}/\partial t$ and $\bar{\mathbf{V}}\cdot\bar{\nabla}\eta$ are shown in Figs. 2a,b. The total horizontal derivative of vorticity $d\bar{\eta}/dt = \partial\bar{\eta}/\partial t + \bar{\mathbf{V}}\cdot\nabla\bar{\eta}$ is shown in Fig. 2c. Generally the vorticity advection by the mean wind $\bar{\mathbf{V}}\cdot\nabla\bar{\eta}$ is positive before the wave trough axis and negative ahead of the ridge axis, contributing to a local increase of the mean vorticity $\bar{\eta}$ with time before the passage of the trough axis and a decrease after the passage of the trough axis. Since convection is weak just before, during, and for some time after the passage of the wave ridge, $d\bar{\eta}/dt$ is slight in wave regions [5] to [R] and [1] to [2]. For these regions of the wave, especially above cloud base and below 300 mb, the local time change of the mean vorticity $\partial\bar{\eta}/\partial t$ and the horizontal advection of the mean vorticity $\bar{\mathbf{V}}\cdot\nabla\bar{\eta}$ are opposite in sign and nearly equal in magnitude. Term $\partial\bar{\eta}/\partial t$ is balanced effectively by $\bar{\mathbf{V}}\cdot\nabla\bar{\eta}$ and $d\bar{\eta}/dt$ is consequently relatively small [~5 to 10 ($\times 10^{-11}\ s^{-2}$)]. Figure 2c shows increased magnitudes of $d\bar{\eta}/dt$ in wave regions [3] and [T] where convective cloud activity is especially strong. In accordance with the simple vorticity equation, just before and during the passage of the trough, cloud-induced convergence and diver-

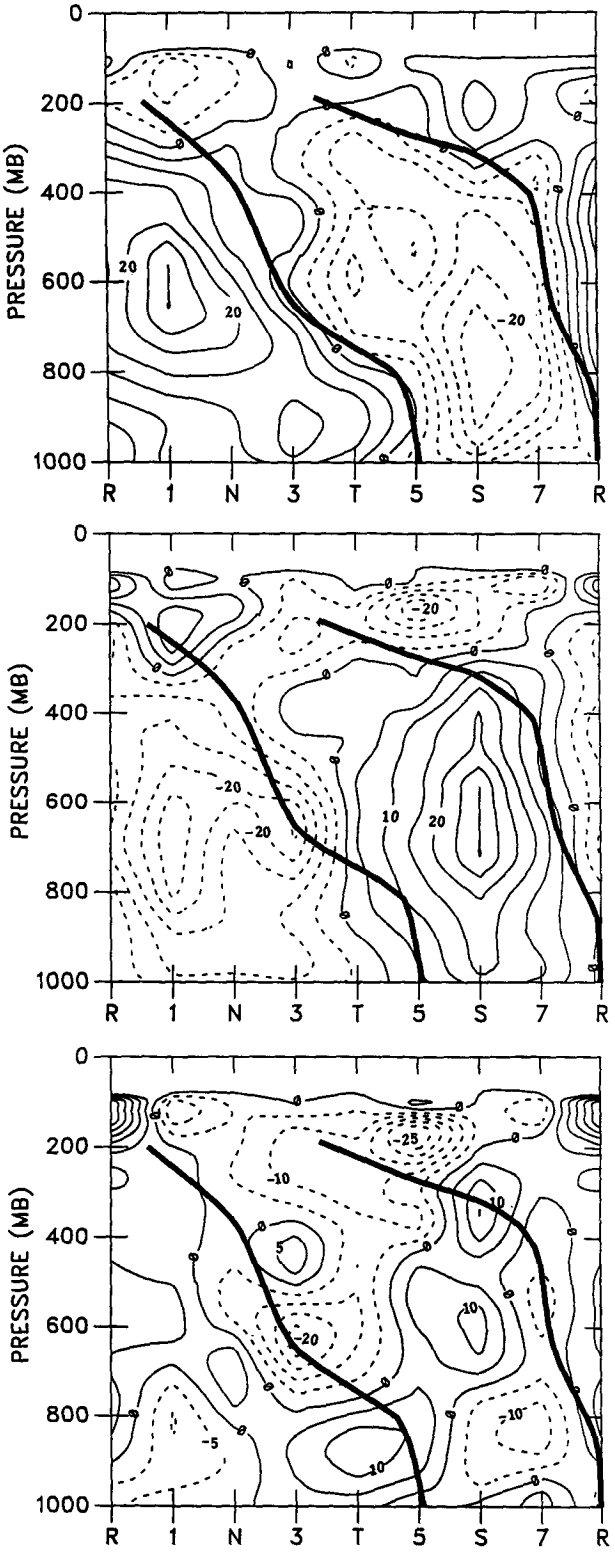

FIG. 2. Vertical cross sections of the (a) local time change of the mean vorticity $\partial\bar{\eta}/\partial t$, (b) horizontal advection of mean vorticity by the mean wind $\bar{\mathbf{V}}\cdot\nabla\bar{\eta}$ and (c) total horizontal derivative of the mean vorticity $d\bar{\eta}/dt$ over one wavelength of the wave. Units: 10^{-11} s^{-2}. The values shown are deviations from the Phase III mean.

gence significantly affects the large-scale vorticity field, substantially altering its evolution.

The wave components of the diagnosed cloud source terms representing the cloud life-cycle effect $\int(\sigma/\tau_{p'})dp'(\bar{\eta}_c-\bar{\eta})$, vortex-tube stretching by cloud scale convergence $-\bar{\eta}(\partial M_c/\partial p)$, and vortex-tube stretching by large-scale convergence $-\bar{\eta}\bar{\delta}$ are shown in Fig. 3. These are three approximately equivalent representations of the cloud effect. There is generally good agreement between the total horizontal derivative of vorticity in Fig. 2c and the cloud source terms in Fig. 3. Here $\int(\sigma/\tau_{p'})dp'(\bar{\eta}_c-\bar{\eta})$, $-\bar{\eta}(\partial M_c/\partial p)$, and $-\bar{\eta}\bar{\delta}$ are seen as quantitatively good estimates of $d\bar{\eta}/dt$ below 300 mb and above cloud base in wave regions [3] and [T], where convection is strongest. Just before and during the passage of the trough, alternating levels of strong apparent vorticity sources and sinks correspond, respectively, to entrainment (convergence) and detrainment (divergence) of environmental air into and out of the cloud ensemble. Generally environmental air is being entrained at lower levels below 750 mb, detrained around 600 mb, entrained again at 400 mb, and detrained again around 200 mb from the cloud ensemble, behavior that corresponds to that of the large-scale mean divergence in Fig. 1b.

There are a few notable discrepancies between $d\bar{\eta}/dt$ and the diagnosed cloud source terms. In general agreement diminishes above 300 mb where the reliability of the dataset decreases, making an accurate determination of $d\bar{\eta}/dt$ and the cloud source terms, which depend on wind and thermodynamic data, difficult. In some wave categories, the poorer agreement above 300 mb appears to be due to unrealistic values of $\partial\bar{\eta}/\partial t$ and $\bar{\mathbf{V}}\cdot\nabla\bar{\eta}$. This is especially true above 200 mb in the ridge region [R] of the wave. Such a large positive vorticity source ($\sim 30\times10^{-11}$ s^{-2}) is unexpected in this region of the wave and is not considered realistic. Comparisons between Figs. 2c and 3 show that, while the diagnosed cloud life-cycle source $\int(\sigma/\tau_{p'})dp'(\bar{\eta}_c-\bar{\eta})$ is a substantially reliable estimate of the behavior of $d\bar{\eta}/dt$ overall, it tends to overestimate the magnitudes of the apparent vorticity sources and sinks in the convectively inactive sectors of the wave. The cloud source terms due to vortex-tube stretching $-\bar{\eta}(\partial M_c/\partial p)$ and $-\bar{\eta}\bar{\delta}$ are seen as better quantitative estimates of $d\bar{\eta}/dt$ in regions of weak convective activity, at least below 400 mb.

5. Vorticity dynamics of tropical easterly waves observed in GATE

Using the composite technique applied to the first-order vorticity equation, it is possible to examine not only the vorticity dynamics of the wave disturbance itself, but the relation between the wave behavior and the basic flow in which it is embedded as well. For this purpose, the large-scale wind, vorticity, and divergence

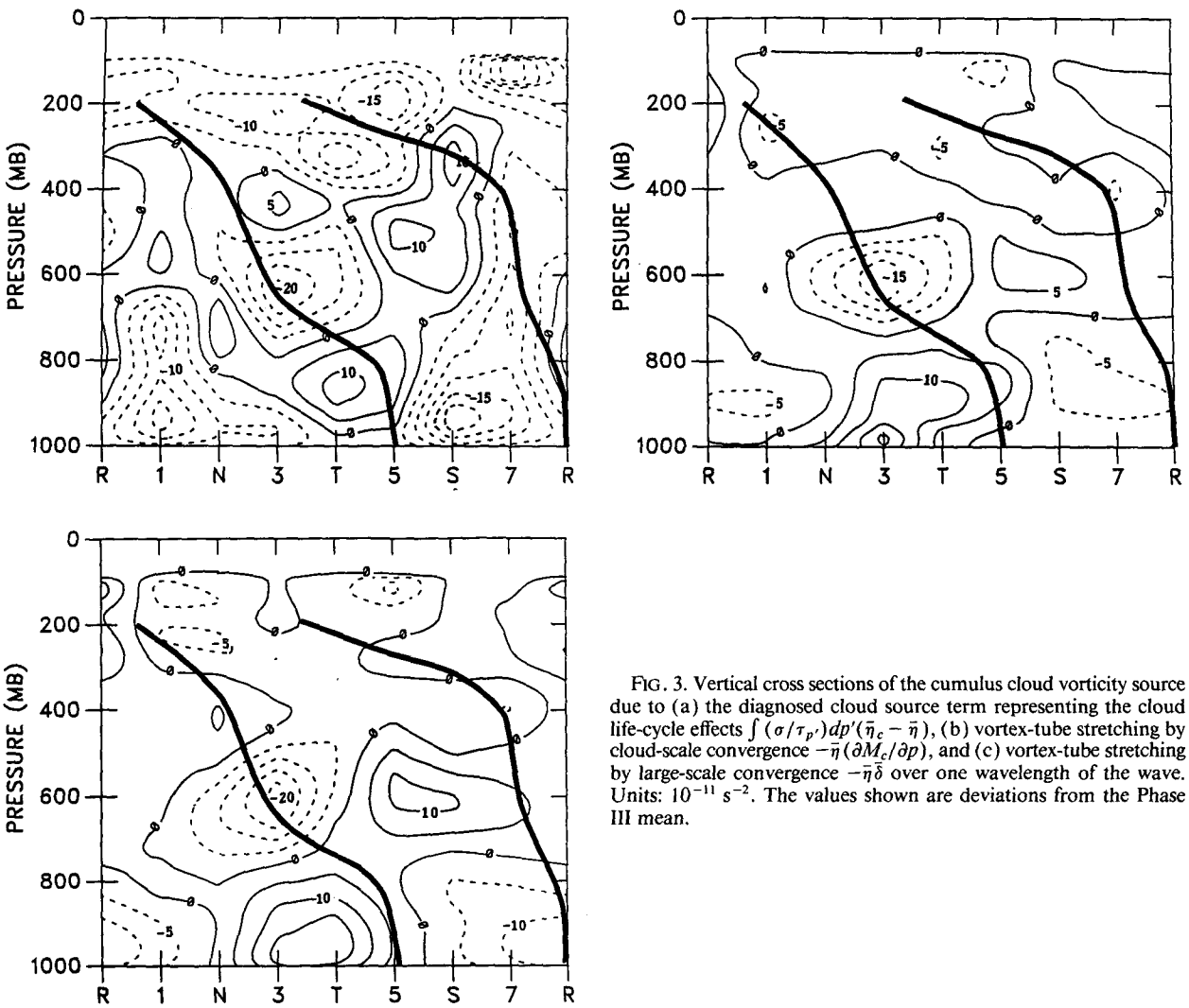

FIG. 3. Vertical cross sections of the cumulus cloud vorticity source due to (a) the diagnosed cloud source term representing the cloud life-cycle effects $\int (\sigma/\tau_{p'})dp'(\bar{\eta}_c - \bar{\eta})$, (b) vortex-tube stretching by cloud-scale convergence $-\bar{\eta}(\partial M_c/\partial p)$, and (c) vortex-tube stretching by large-scale convergence $-\bar{\eta}\bar{\delta}$ over one wavelength of the wave. Units: 10^{-11} s^{-2}. The values shown are deviations from the Phase III mean.

fields are decomposed into zonal means plus deviations from the zonal mean:

$$\left.\begin{aligned}\bar{\mathbf{V}} &= \langle \mathbf{V} \rangle + \hat{\mathbf{V}} \\ \bar{\eta} &= \langle \eta \rangle + \hat{\eta} \\ \bar{\delta} &= \langle \delta \rangle + \hat{\delta}\end{aligned}\right\}. \tag{5}$$

Zonally averaged fields are bracketed by $\langle \cdot \rangle$ and deviations from the zonal means are denoted by the accent ($\hat{\ }$). Consistent with the compositing technique, the zonal mean velocity field is constant in time. Substituting (5) into (3) yields

$$\frac{\partial \hat{\eta}}{\partial t} + \langle \mathbf{V} \rangle \cdot \nabla \hat{\eta} + \hat{\mathbf{V}} \cdot \nabla \langle \eta \rangle + \hat{\mathbf{V}} \cdot \nabla \hat{\eta} + \langle \mathbf{V} \rangle \cdot \nabla \langle \eta \rangle = -\langle \eta \rangle \hat{\delta} - \langle \eta \rangle \langle \delta \rangle - \hat{\eta}\hat{\delta} - \hat{\eta}\langle \delta \rangle, \tag{6}$$

where

$$\langle \mathbf{V} \rangle \cdot \nabla \hat{\eta} = \langle u \rangle \frac{\partial \hat{\eta}}{\partial x} + \langle v \rangle \frac{\partial \hat{\eta}}{\partial y},$$

$$\hat{\mathbf{V}} \cdot \nabla \langle \eta \rangle = \hat{u} \left\langle \frac{\partial \eta}{\partial x} \right\rangle + \hat{v} \left\langle \frac{\partial \eta}{\partial y} \right\rangle,$$

$$\hat{\mathbf{V}} \cdot \nabla \hat{\eta} = \hat{u} \frac{\partial \hat{\eta}}{\partial x} + \hat{v} \frac{\partial \hat{\eta}}{\partial y},$$

and

$$\langle \mathbf{V} \rangle \cdot \nabla \langle \eta \rangle = \langle u \rangle \left\langle \frac{\partial \eta}{\partial x} \right\rangle + \langle v \rangle \left\langle \frac{\partial \eta}{\partial y} \right\rangle.$$

Here u and v are the east–west and north–south wind components of the horizontal wind vector $\mathbf{V}$.

It is seen in Figs. 2a, 4a,b that the effects of the local time change of the perturbed vorticity $\partial\hat{\eta}/\partial t$, the advection of the perturbed vorticity by the mean zonal wind $\langle \mathbf{V} \rangle \cdot \nabla \hat{\eta}$, and the advection of the zonal mean vorticity by the perturbed wind $\hat{\mathbf{V}} \cdot \nabla \langle \eta \rangle$ are substantial, with amplitudes ranging from ~ 15 to 30×10^{-11} s^{-2}. Since the magnitudes of the zonal mean wind $\langle u \rangle$ and $\langle \partial\eta/\partial y \rangle$ are so large, the advection of the perturbed vorticity $\langle \mathbf{V} \rangle \cdot \nabla \hat{\eta}$ is primarily due to $\langle u \rangle \partial\hat{\eta}/\partial x$, and $\hat{v}\langle \partial\eta/\partial y \rangle$ effectively determines the entire effect of the advection of the zonal mean vorticity $\hat{\mathbf{V}} \cdot \nabla \langle \eta \rangle$. The advection of the zonal mean vorticity by the zonal mean wind $\langle \mathbf{V} \rangle \cdot \nabla \langle \eta \rangle$ is not large, and its relative contribution to (6) is not substantial, being only one-fifth the strength of $\partial\hat{\eta}/\partial t$.

The nonlinear advective term $\hat{\mathbf{V}} \cdot \nabla \hat{\eta}$ (not shown) is computed to be small. Overall the magnitude of $\hat{\mathbf{V}} \cdot \nabla \hat{\eta}$ is less than one-fifth that of $\partial\hat{\eta}/\partial t$. Although the individual advective terms that constitute $\hat{\mathbf{V}} \cdot \nabla \hat{\eta}$ are quite large ($\hat{u}\partial\hat{\eta}/\partial x$, $\hat{v}\partial\hat{\eta}/\partial y \sim 10$ to 15×10^{-11} s^{-2}), almost complete cancellation occurs between them with the net result being practically negligible $\hat{\mathbf{V}} \cdot \nabla \hat{\eta}$ values. This is a consequence of the easterly wave behaving like a quasi-nondivergent single sinusoidal wave throughout virtually its entire height and length at this stage of its development.

The contributions made by $-\hat{\eta}\hat{\delta}$ and $-\hat{\eta}\langle \delta \rangle$ (not shown) are considerably smaller than any other term on the right side of (6). Only slightly appreciable negative values ($\sim 5 \times 10^{-11}$ s^{-2}) of the nonlinear vortex-tube stretching $-\hat{\eta}\hat{\delta}$ occur at 600 mb in wave category [3], just before the trough, where cumulus activity is strong. The zonal mean divergence $\langle \delta \rangle$ and perturbation $\hat{\delta}$ are of the order $\sim 5 \times 10^{-6}$ s^{-1}, with $\hat{\delta}$ being generally somewhat greater than $\langle \delta \rangle$. The zonal mean absolute vorticity $\langle \eta \rangle$ is mainly responsible for the relatively larger contributions by $-\langle \eta \rangle \langle \delta \rangle$ (not shown) and $-\langle \eta \rangle \hat{\delta}$ (Fig. 4c) in (6).

Based on the previous discussion, the easterly wave can be described approximately by a linearized form of (6):

$$\frac{\partial\hat{\eta}}{\partial t} + \langle \mathbf{V} \rangle \cdot \nabla \hat{\eta} + \hat{\mathbf{V}} \cdot \nabla \langle \eta \rangle \approx -\langle \eta \rangle \hat{\delta} \qquad (7)$$

where only the dominate terms are kept and the contribution from the basic flow is subtracted out. To check how well (7) approximates the balance between the temporal and spatial evolution of the wave vorticity and the cloud-induced large-scale divergence, Fig. 5 shows the perturbed divergence $\hat{\delta}$ obtained from (7) and it is compared to the observed wave divergence in Fig. 1b. Equation (7) does produce the correct outline of major regions of convergence and divergence, even though there are some differences in the shape of the contours. Below 300 mb the agreement is quantitatively acceptable as well over most regions of the wave. Above

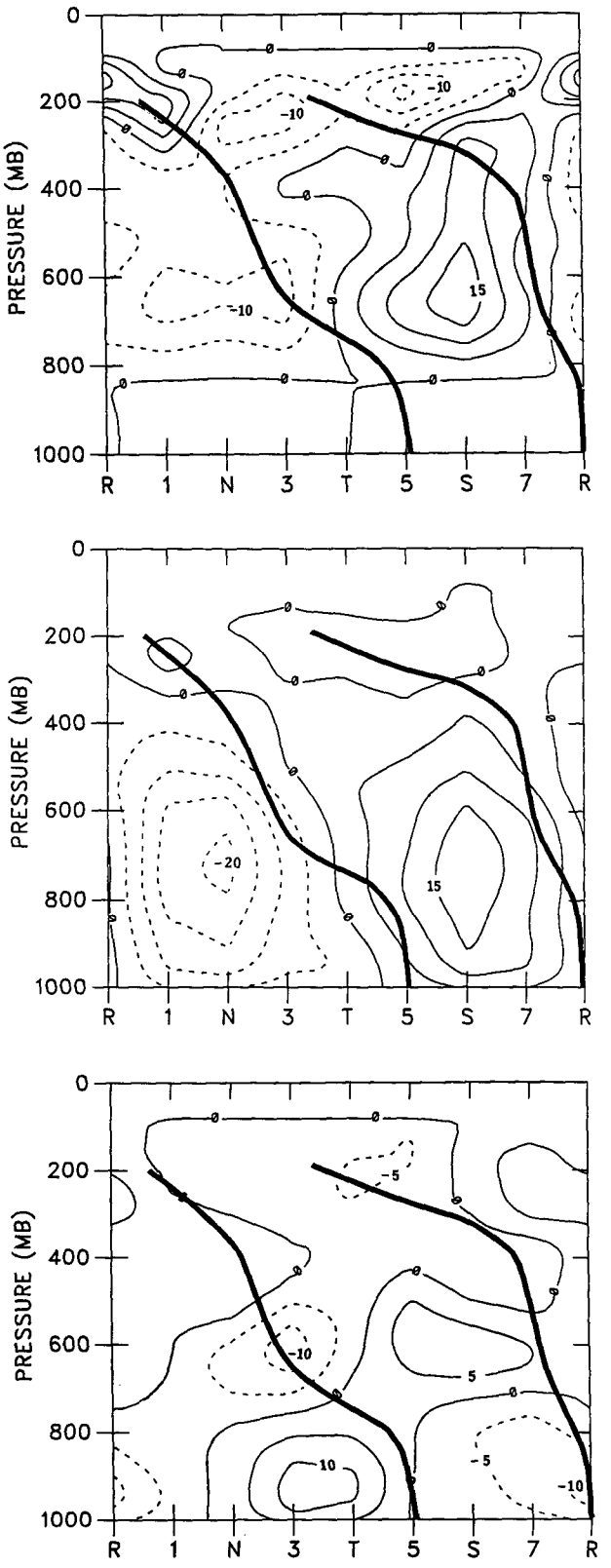

FIG. 4. Vertical cross sections of (a) $\langle \mathbf{V} \rangle \cdot \nabla \hat{\eta}$, (b) $\hat{\mathbf{V}} \cdot \nabla \langle \eta \rangle$, and (c) $-\langle \eta \rangle \hat{\delta}$ over one wavelength of the wave. Units: 10^{-11} s^{-2}.

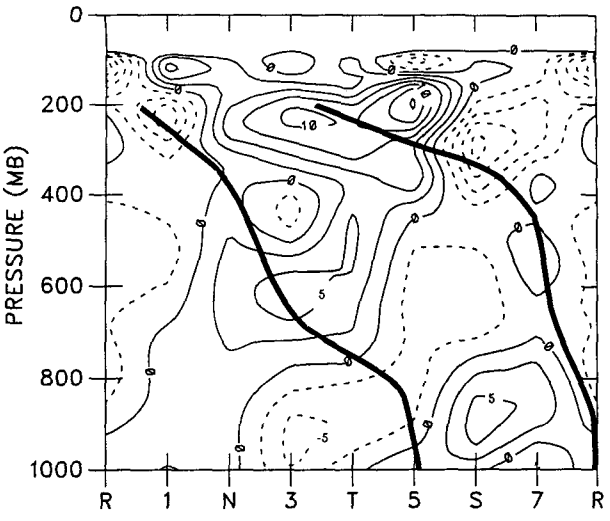

FIG. 5. Vertical cross sections of the perturbed divergence $\hat{\delta}$ given by (7) the linearized approximate form of the simple vorticity equation over one wavelength of the wave. Units: 10^{-6} s^{-1}.

300 mb however there are major discrepancies in magnitude. Figure 5 shows considerably larger centers of convergence and divergence than those observed.

We can interpret the observed structure of the composite easterly wave using a single sine wave representation for a typical tropical easterly wave where the local change of wave vorticity is dominated by the propagational translation of the perturbed vorticity. Assuming a steady-state wave propagating with a constant zonal phase velocity $\mathbf{C}$, the local time change and advection of the perturbed vorticity by the zonal mean wind $\langle \mathbf{V} \rangle$ can be combined and (7) rewritten as

$$(\langle \mathbf{V} \rangle - \mathbf{C}) \cdot \nabla \hat{\eta} + \hat{\mathbf{V}} \cdot \nabla \langle \eta \rangle \approx -\langle \eta \rangle \hat{\delta}. \quad (8)$$

Equation (8) now implies a direct relationship between the wave divergence and the net effect of two advection processes, the advection of the perturbed vorticity by the relative zonal mean wind, and the advection of the zonal mean vorticity by the perturbed wind.

For easterly waves observed during Phase III of GATE, the relative advecting wind was westerly up to ~280 mb (Thompson et al. 1979; Fig. 3). If a single sinusoidal wave is a reasonable representation of a composite easterly wave, it is expected that below 280 mb the advection of the perturbed vorticity by the relative zonal mean wind $(\langle \mathbf{V} \rangle - \mathbf{C}) \cdot \nabla \hat{\eta}$ behaves similarly to that of $\hat{\eta}$ but shifted westward by approximately one-quarter of a wavelength. Figure 6a is the combination of Figs. 2a and 4a, and represents the effect of $(\langle \mathbf{V} \rangle - \mathbf{C}) \cdot \nabla \hat{\eta}$. West (east) of the trough axis, negative (positive) advection of perturbed vorticity by the zonal mean wind is observed up to the 280-mb level, in accord with a single sine wave representation. Likewise, the advection of the zonal mean vorticity by the perturbed wind $\hat{\mathbf{V}} \cdot \nabla \langle \eta \rangle$ shown in Fig. 6b is similar in behavior to that of $\hat{\eta}$ but shifted eastward by approximately one-quarter of a wavelength. Positive (negative) advection of zonal mean vorticity by the perturbed wind occurs west (east) of the trough axis.

The synoptic-scale features dictate which advection process dominates the vorticity dynamics to produce the observed wave divergence in Fig. 1b. The influence of the strong low-level monsoon westerlies is seen in Fig. 6a, where especially large positive values of $(\langle \mathbf{V} \rangle - \mathbf{C})$ result in particularly large amplitudes of negative and positive advection of perturbed vorticity by the relative zonal mean wind below 800 mb. Corresponding strong low-level wave convergence is observed between regions $[N]$ and $[T]$, and divergence between regions [5] and $[R]$. Above 800 mb the magnitude of the relative wind $(\langle \mathbf{V} \rangle - \mathbf{C})$ during Phase III of GATE is decreased and the magnitude of the perturbed wind compared to the zonal mean is correspondingly increased. The influence of the southward extension of the midtropospheric easterly jet centered near 15°N over Africa in the summer is seen in Fig. 6b. Because $\langle \partial \eta / \partial y \rangle$ is positive and especially large between 600 and 700 mb during Phase III of GATE, and perturbation $\hat{v}$ peaks at ±5 m s^{-1} there, relatively substantial positive and negative advections of mean zonal vorticity by the perturbed wind $\hat{\mathbf{V}} \cdot \nabla \langle \eta \rangle$ are observed in this layer of the troposphere. At the level of the African easterly jet $\langle u \rangle$ reaches larger negative values, diminishing somewhat the contribution by $(\langle \mathbf{V} \rangle - \mathbf{C}) \cdot \nabla \hat{\eta}$. Consequently corresponding wave divergence and convergence maxima occur above regions $[N]$ and $[S]$, west and east of the trough axis, respectively, at these levels. Using the single sine wave representation, the influence on the wave divergence of (a) the advection of perturbed vorticity by the relative zonal mean wind below 800 mb and (b) the advection of zonal mean vorticity by the perturbed wind in the midtroposphere are indicated schematically in Fig. 7. Above 500 mb the influence of the advection of mean zonal vorticity by the perturbed wind diminishes, and the vorticity dynamics are again dominated by the advection of the perturbed vorticity by the relative zonal mean wind (Fig. 6a). Convergence is observed just before the trough, divergence before the ridge.

It appears that above 280 mb, where the relative motion is to the west, the simple picture of a steady-state quasi-nondivergent sinusoidal wind component presented in Fig. 7 is no longer applicable. This may be because the magnitude of the wind perturbations is large and the amplitudes of the wave divergence are comparable to vorticity, or, as mentioned previously, the data are not reliable.

6. Concluding remarks

We have presented in this paper some observational evidence that suggests that Cho et al's. (1983) first-

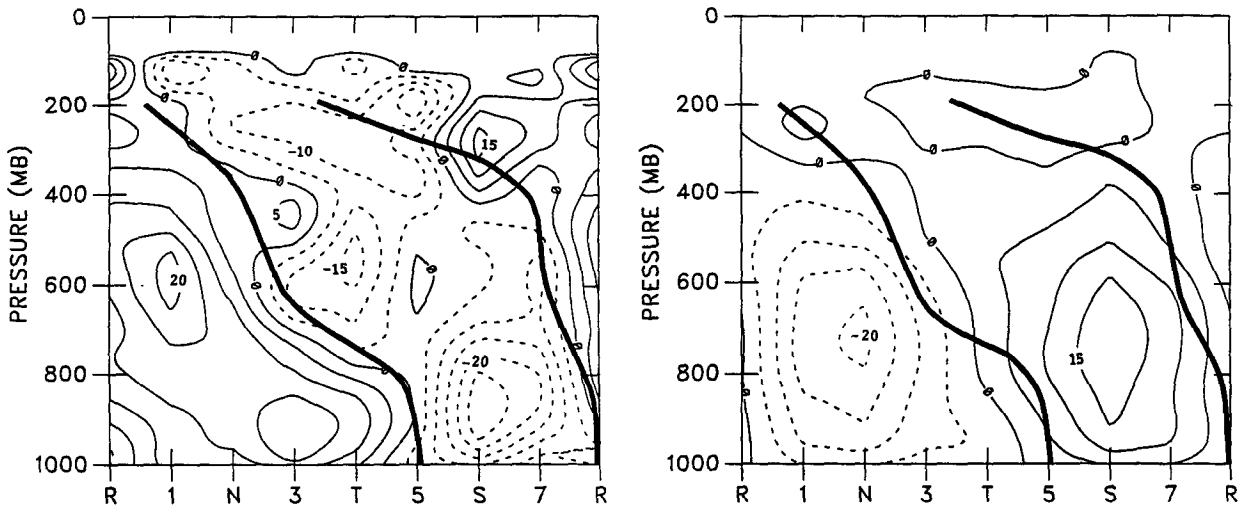

FIG. 6. Vertical cross sections of (a) $\partial\hat{\eta}/\partial t + \langle \mathbf{V} \rangle \cdot \nabla\hat{\eta}$ and (b) $\hat{\mathbf{V}} \cdot \nabla\langle\eta\rangle$ over one wavelength of the wave. Units: 10^{-11} s^{-2}.

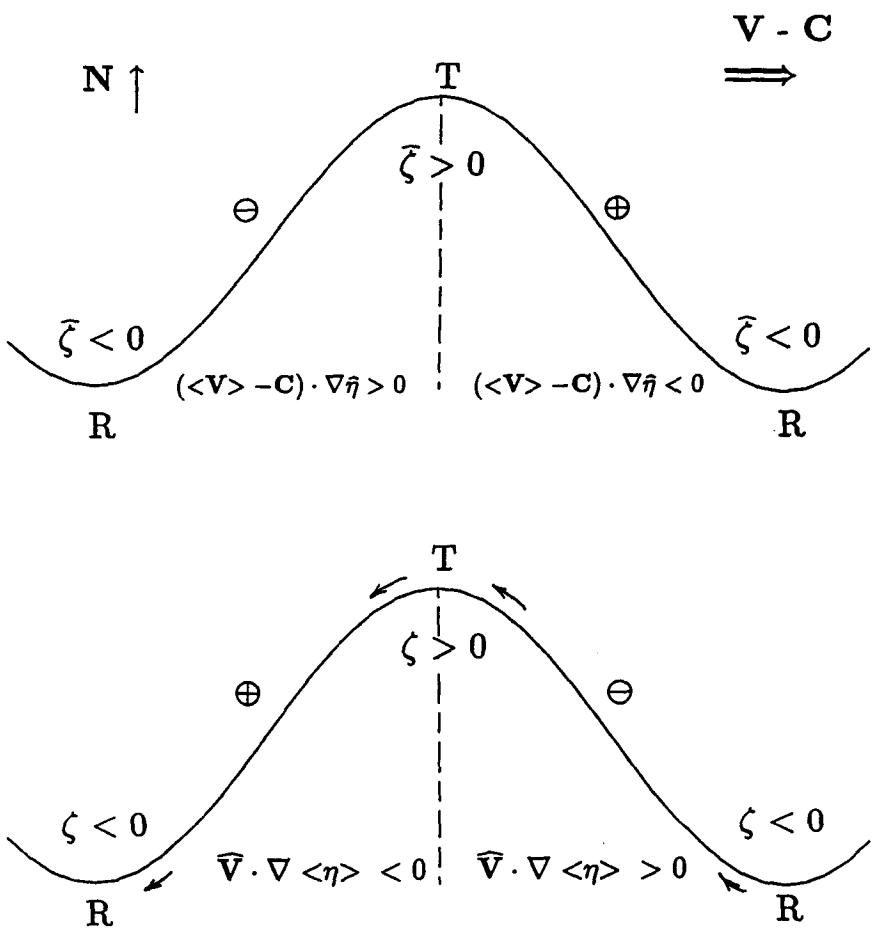

FIG. 7. Schematic easterly wave showing regions of positive and negative advections of (a) the perturbed vorticity by the relative zonal mean wind, and (b) the zonal mean vorticity by the perturbed wind. (←) indicates wind direction, (⇒) direction of wave motion, ⊕ related wave divergence, and ⊖ wave convergence.

order vorticity equation can account for the vorticity dynamics of tropical easterly waves, at least in the diagnostic sense. The consistency between the profiles and cross sections given for comparison is reasonably good and the composite budgets show that the first-order vorticity equation can reproduce the observed vorticity dynamics of the tropical easterly waves that passed over GATE during Phase III in all, both convectively active and inactive, sectors of these disturbances.

The first-order vorticity equation implies a direct correspondence between the convergence and divergence of the total cloud mass flux and the evolution of the large-scale tropical vorticity field. For adiabatic tropical circulations, free of convective clouds, the vorticity source due to cumulus convection vanishes, the mean divergence is generally weaker than the mean vorticity field, and synoptic-scale disturbances can be described as simple Rossby-type waves. However, our results indicate that in tropical disturbances of strong convective activity, cloud-induced vortex-tube stretching, reflected on the synoptic scale as the convergence of the mean wind, acts as an apparent vorticity source and contributes to the evolution of the mean vorticity field, significantly altering the wave structure. The properties of this vorticity wave differ from those of a simple Rossby wave in two respects. First, the stretching of vortex tubes by cumulus cloud has a strong effect on the evolution of the mean vorticity field. Second, due to cloud induced divergence the mean horizontal wind contains both a solenoidal component and an irrotational component.

Also according to the composite analysis of the first-order vorticity equation, the terms that most strongly influence the behavior of the perturbed divergence of a tropical easterly wave are the competing effects of the advection of perturbed vorticity by the relative zonal mean wind and the advection of the zonal mean vorticity by the perturbed wind. Using an idealized single sine wave representation where the local change of wave vorticity is dominated by the propagational translation of the perturbed vorticity, the observed behavior of the wave divergence is physically interpreted and a comparatively straightforward explanation for the dynamic equilibrium maintained by easterly waves during Phase III of GATE is presented. It is found that the environmental wind characteristic of Phase III of GATE is responsible for the complex wave divergence pattern. The strong wave convergence observed just before the passage of the surface trough is associated with the low-level westerly monsoon flow over western Africa during the summer, and the middle-level wave divergence maximum seen just before the trough axis is related to the midtropospheric easterly African jet and strong meridional wind fluctuations.

As the analysis shows, the simplicity of Cho et al.'s (1983) first-order vorticity equation not only makes it possible to identify and explain what effects are essential to the vorticity dynamics of tropical easterly waves during this stage of their development, but suggests the possibility of future prognostic use to study the evolution and intensification of large-scale tropical circulation systems, provided the cloud-source term can be specified.

As discussed by Cho et al. (1983), the substitution of $\bar{\eta}$ for $\bar{\eta}_{CB}$ in (2) and (3) is equivalent to the assumption that the effect of horizontal eddy transport of absolute vorticity is negligible. The observa-eqtional evidence suggests that the diagnosed values of $\int (\sigma/\tau_{p'}) dp'(\bar{\eta}_c - \bar{\eta})$, $-\bar{\eta}(\partial M_c/\partial p)$, and $-\bar{\eta}\bar{\delta}$ are all-good estimates of the cloud effect, and that the approximation of $\bar{\eta}$ for $\bar{\eta}_{CB}$ is quantitatively reliable to a substantial degree. This agrees with Cho et al.'s (1983) previous finding that these three representations appear to give essentially the same results. Future studies using dynamic three-dimensional time-dependent cloud models to independently determine these parameters are suggested in order to properly understand and incorporate the effects of convection into the first-order dynamics of tropical easterly waves.

Acknowledgments. This work was supported by research grants from the Natural Sciences and Engineering Research Council of Canada and the Canadian Atmospheric Environment Service. The comments from two anonymous reviewers are appreciated.

REFERENCES

Cheng, L., T.-C. Yip and H.-R. Cho, 1980: Determination of mean cumulus cloud vorticity from GATE *A/B*-scale potential vorticity budget. *J. Atmos. Sci.*, **37**, 797–811.

Cho, H.-R., 1977: Contribution of cumulus cloud life-cycle effects to the large-scale heat and moisture budget equations. *J. Atmos. Sci.*, **34**, 87–97.

——, and L. Cheng, 1980: Parameterization of horizontal transport of vorticity by cumulus convection. *J. Atmos. Sci.*, **37**, 812–826.

——, and T. L. Clark, 1981: A numerical investigation of the structure of vorticity fields associated with a deep convective cloud. *Mon. Weather Rev.*, **109**, 1654–1670.

——, L. Cheng and R. M. Bloxam, 1979: The representation of cumulus cloud effects in the large-scale vorticity equation. *J. Atmos. Sci.*, **36**, 127–139.

——, M. A. Jenkins and J. Boyd, 1983: A first-order vorticity equation for tropical easterly waves. *J. Atmos. Sci.*, **40**, 958–968.

Chu, J.-H., M. Yanai and C.-H. Sui, 1981: Effects of cumulus convection on the vorticity field in the tropics. Part I: The large-scale budget. *J. Meteor. Soc. Japan*, **59**, 535–546.

Daggupatty, S. M., and D. R. Sikka, 1977: On the vorticity budget and vertical velocity distribution associated with the life-cycle of a monsoon depression. *J. Atmos. Sci.*, **34**, 773–792.

Jenkins, M. A., R. M. Bloxam and H.-R. Cho, 1982: Further test of a theory of convective effects on the large-scale vorticity field in the tropics. *Atmos. Ocean*, **20**, 207–226.

Johnson, R. H., 1976: The role of convective-scale precipitation downdraft in cumulus and synoptic-scale interactions. *J. Atmos. Sci.*, **33**, 1890–1910.

Nitta, T., 1977: Response of cumulus updraft and downdraft to GATE *A/B*-scale motion systems. *J. Atmos. Sci.*, **34**, 1163–1186.

——, 1977: The effects of cloud detrainment on the diagnosed properties of cumulus properties. *J. Atmos. Sci.*, **34**, 359–366.

Reed, R. J., and E. E. Recker, 1971: Structure and properties of synoptic-scale wave disturbances in the equatorial western Pacific. *J. Atmos. Sci.*, **28,** 1117–1133.

——, and R. H. Johnson, 1974: The vorticity budget of synoptic-scale wave disturbances in the tropical western Pacific. *J. Atmos. Sci.*, **31,** 1784–1790.

——, D. C. Norquist and E. E. Recker, 1977: The structure and properties of African wave disturbances as observed during Phase III of GATE. *Mon. Weather Rev.*, **105,** 317–333.

Ruprecht, E., and W. M. Gray, 1976: Analysis of satellite-observed tropical clusters. I. Wind and dynamic fields. *Tellus,* **29,** 391–413.

Shapiro, L. J., 1978: The vorticity budget of a composite African tropical wave disturbance. *Mon. Weather Rev.*, **106,** 806–817.

——, and D. E. Stevens, 1980: Parameterization of convective effects on the momentum and vorticity budgets of synoptic-scale Atlantic tropical waves. *Mon. Weather Rev.*, **108,** 1816–1826.

Stevens, D. E., 1979: Vorticity, momentum and divergence budgets of synoptic-scale wave disturbances in the tropical eastern Atlantic. *Mon. Weather Rev.*, **107,** 535–550.

Sui, C.-H., and M. Yanai, 1986: Cumulus ensemble effects on the large-scale vorticity and momentum fields of GATE. Part I: Observational evidence. *J. Atmos. Sci.*, **43,** 1618–1642.

——, M.-D. Cheng, X. W and M. Yanai, 1989: Cumulus ensemble effects on the large-scale vorticity and momentum fields of GATE. Part II: Parameterization. *J. Atmos. Sci.*, **46,** 1609–1629.

Thompson, R. M., Jr., S. W. Payne, E. E. Recker and R. J. Reed, 1979: Structure and properties of synoptic-scale wave disturbances in the intertropical convergence zone of the eastern Atlantic. *J. Atmos. Sci.*, **36,** 53–72.

Williams, K. T., and W. M. Gray, 1973: Statistical analysis of satellite-observed trade wind cloud clusters in the western north Pacific. *Tellus,* **25,** 313–336.

Yanai, M., and T. Nitta, 1967: Computation of vertical motion and vorticity budget in a Caribbean easterly wave. *J. Meteor. Soc. Japan,* **45,** 444–466.

——, C.-H. Sui and J.-H. Chu, 1982: Effects of cumulus convection on the vorticity field in the tropics. Part I: The large-scale budget. *J. Meteor. Soc. Japan,* **59,** 535–546.

——, ——, and ——, 1982: Effects of cumulus convection on the vorticity field in the tropics. Part II: Interpretation. *J. Meteor. Soc. Japan,* **60,** 411–423.